

Conditional Motional Squeezing of an Optomechanical Oscillator Approaching the Quantum Regime

Benjamin B. Lane^{1†}, Junxin Chen^{1†}, Ronald E. Pagano²,
Scott Aronson², Garrett D. Cole³, Xinghui Yin¹, Thomas
R. Corbitt², Nergis Mavalvala^{1*}

^{1*}LIGO, Massachusetts Institute of Technology, 185 Albany Street,
Cambridge, Massachusetts, 02139, USA.

²Department of Physics and Astronomy, Louisiana State University,
Tower Drive, Baton Rouge, Louisiana, 70803, USA.

³Thorlabs Crystalline Solutions, 114 E Haley St., Suite G, Santa
Barbara, California, 93101, USA.

*Corresponding author(s). E-mail(s): nergis@ligo.mit.edu;

†These authors contributed equally to this work.

Abstract

Squeezed mechanical states are a valuable tool for quantum sensing and error correction in quantum computing, and a pivotal platform for tests of fundamental physics. Recently, solid state mechanical oscillators have been prepared in squeezed states using parametric interactions in both the microwave and optical regimes. It has long been predicted that a fast measurement rate comparable to the mechanical resonance frequency can prepare the oscillator under measurement into a quantum squeezed state. Despite decades of effort, this straightforward protocol is yet to be demonstrated in the quantum regime. Here, we use post-processing techniques to demonstrate preparation of a **50** ng GaAs cantilever in a conditional classical squeezed state with a minimum uncertainty (**0.28±0.18**) dB above (**1.07±0.04** times) the zero point fluctuations, **3** orders of magnitude closer to the quantum regime in variance than the previous record. This paves the way

to real-time measurement-based preparation of macroscopic oscillators in quantum squeezed states, and can be adapted to mechanical systems as large as the kg-scale test masses of the Laser Interferometer Gravitational-Wave Observatory (LIGO).

Keywords: macroscopic quantum state preparation, quantum optomechanics, quantum state estimation

A quantum squeezed state is characterized by exhibiting one quadrature with uncertainty less than that of the zero point fluctuation (ZPF), at the expense of larger uncertainty in the conjugate quadrature. In the squeezed quadrature, measurement of a physical quantity is subjected to less noise than the corresponding unsqueezed ground state. Due to this noise reduction, for a mechanical system, the generation and observation of a quantum squeezed state is expected to provide a substantial resource for quantum sensing and quantum metrology [1–3], and for error correction in quantum computing [4, 5]. Furthermore, due to the relatively large mass of solid-state mechanical oscillators, mechanical quantum squeezed states are also a promising probe of the quantum-to-classical transition [6–9], and test of quantumness of gravity [10].

The key to preparing mechanical quantum squeezed states is to violate the equipartition of energy between the displacement \hat{q} and the momentum \hat{p} quadratures. Solid state mechanical oscillators have first been prepared in quantum squeezed states using reservoir engineering on microwave devices [11–14]. By introducing coupling to superconducting qubits, non-Gaussian quantum squeezed states have been successfully prepared [15, 16]. In the optical domain, direct migration of the reservoir engineering technique to optical devices has achieved back-action evasion, but fell short of quantum squeezed state preparation due to excess noise such as optical heating [17]. Instead, inspired by ion trapping techniques [18], where quantum squeezed mechanical states are prepared by modulating the trapping potential, quantum squeezed center-of-mass motion of a particle levitated in laser fields was inferred after subtracting readout

noise [19]. So far, all successful demonstrations of mechanical quantum squeezed state preparation can be classified as utilizing parametric interactions.

Another avenue for preparing mechanical quantum states is a continuous measurement-based preparation scheme, which has the advantage of simpler and steadier experimental control. This not only allows for a simplified experimental setup, but would also be directly applicable to complex instruments such as LIGO to avoid catastrophic instability. Feedback cooling of mechanical oscillators to the ground state using measurement rates faster than the thermal decoherence rate has already been achieved [20–22]. However, in these demonstrations, the equipartition of energy in the displacement and momentum quadratures is preserved due to the much faster mechanical oscillations compared to the measurement rates. In this regime, the rotating wave approximation is valid, precluding the preparation of squeezed states. It has been predicted more than two decades ago that a measurement rate Γ_{meas} comparable or faster than the resonance frequency of the mechanical oscillator Ω_{m} can violate equipartition, and thus, allow for preparation of quantum squeezed states [23]. This approach has been refined over the last decades by incorporating state estimation and conditional state preparation [24, 25].

Measurement-Based Preparation of Mechanical Squeezed State

State estimation is a broadly used technique to extract a physical observable from a noisy measurement. It plays a pivotal role in our work. Here, we briefly introduce the concepts of state estimation and the conditional state of a mechanical oscillator to lay the foundation for subsequent discussions. For any linear continuous measurement of displacement \hat{q} , the measurement outcome has the form $\mu\hat{q} + \nu$, with μ a factor expressing the strength of the measurement and ν the imprecision noise. The measurement outcome can be normalized to displacement units by dividing by μ as

$\hat{y}(t) = \hat{q}(t) + \hat{z}(t)$, where $\hat{z}(t)$ is the normalized measurement imprecision noise. The measurement process perturbs the mechanical system, and adds noise to \hat{q} , which is referred as quantum back-action. A typical source of quantum back-action noise is the random momenta transferred from photons in the measurement apparatus to the mechanical oscillator [2, 20]. To extract $\hat{q}(t)$ from a noisy measurement record $\hat{y}(t)$, an estimation filter $H_q(t)$ can be constructed and applied using a priori knowledge of the system, such as system parameters and noise spectra [26–28]. The estimator of displacement is subsequently given by $\hat{q}_e(t) = H_q * \hat{y}(t)$, with $*$ denoting convolution. Due to contamination of the signal by imprecision noise \hat{z} and back-action noise, the estimator \hat{q}_e always deviates from the true value \hat{q} . The error of the estimate can be written as $\delta\hat{q}(t) = \hat{q}(t) - \hat{q}_e(t)$. One can similarly define \hat{p}_e and $\delta\hat{p}$ for momentum \hat{p} . For a linear system driven by stationary Gaussian noise, it is well known that the Wiener filters minimize the mean square of estimation errors [26].

For Gaussian states, the mean values of the estimators $\langle \hat{q}_e \rangle$ and $\langle \hat{p}_e \rangle$ and the (co-)variances of their corresponding errors $V_{\delta q \delta q}$, $V_{\delta p \delta p}$ and $C_{\delta q \delta p}$ uniquely define a state centered at the mean values in phase space with uncertainties given by the estimation errors [24, 25, 29]. As the estimators and estimation errors depend on the measurement record \hat{y} , the state is deemed a conditional state. The mean values directly inherit the stochastic nature of the measurement record $\hat{y}(t)$, resulting in a random walk of the conditional state center in phase space, within the distribution of a thermal state given by the thermal and back-action baths, as shown in Fig. 1(a). On the contrary, the variances of the estimation errors decrease deterministically in time, and converge to a steady state value, as more information is extracted from the measurement process [28]. The steady state value is determined by measurement rate Γ_{meas} , thermal decoherence rate Γ_{th} and back-action rate Γ_{ba} shown in Fig. 1(b) and the mechanical frequency Ω_m shown in Fig. 1(c). A conditional state prepared by causal filters (constructed using past information) can be transferred into an unconditional

state through feedback in real time [30]. On the other hand, due to the requirement of future information, a conditional state prepared by non-causal filters is not accessible in real time, and cannot be transferred to an unconditional state by feedback. Moreover, non-causal filters may result in unphysical conditional states, which violates the Heisenberg uncertainty principle [31]. Therefore, for measurement-based preparation of physical mechanical states, estimate filters should be causal. In addition, to minimize the uncertainty, causal Wiener filters are the typical choices of H_q and H_p . We follow this practice in our work.

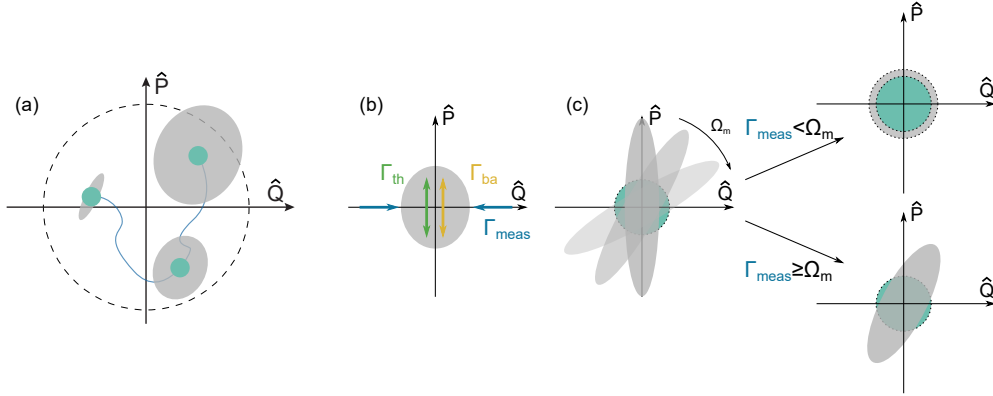


Fig. 1: (a) Evolution of a conditional state. The axes are in dimensionless units defined as $\hat{Q} = \hat{q}/2q_{\text{zpf}}$ and $\hat{P} = \hat{p}/2p_{\text{zpf}}$, with $q_{\text{zpf}} = \sqrt{\hbar/2m\Omega_m}$ and $p_{\text{zpf}} = \sqrt{\hbar m\Omega_m/2}$, where m is the effective mass and Ω_m is the mechanical resonance frequency. The gray shade represents the estimation errors (i.e. the uncertainties of the conditional state), the green circle indicates the magnitude of the ZPF, and the dashed circle represents the thermal distribution. The center of the conditional state goes through a random walk, while the uncertainties reduce deterministically, converging to a steady state. (b) The uncertainties of the conditional state. Thermal decoherence rate Γ_{th} and back-action rate Γ_{ba} increases the uncertainty in the momentum quadrature, while the measurement rate Γ_{meas} decreases the uncertainty in the displacement quadrature. (c) The effect of quadrature rotation on the uncertainties of the conditional state.

Now we discuss how the rates and mechanical frequency influence the steady state estimation errors. The Heisenberg-Langevin equations for a cavity optomechanical

system are

$$\dot{\hat{X}}(t) = -\frac{\kappa}{2}\hat{X}(t) - \Delta\hat{Y}(t) + \sqrt{\kappa}\hat{X}_{\text{in}}(t) \quad (1)$$

$$\dot{\hat{Y}}(t) = -\frac{\kappa}{2}\hat{Y}(t) + \Delta\hat{X}(t) + \sqrt{2}G\alpha\hat{q}(t) + \sqrt{\kappa}\hat{Y}_{\text{in}}(t) \quad (2)$$

$$\dot{\hat{q}}(t) = \frac{\hat{p}(t)}{m} \quad (3)$$

$$\dot{\hat{p}}(t) = -m\Omega_{\text{m}}^2\hat{q}(t) + \sqrt{2}\hbar G\alpha\hat{X}(t) - \Gamma_{\text{m}}\hat{p}(t) + \hat{\xi}_{\text{th}}(t), \quad (4)$$

where \hat{X} and \hat{Y} are the amplitude and phase fluctuations of the intra-cavity optical field respectively; κ is the angular cavity linewidth; Δ is the angular cavity detuning; \hat{X}_{in} and \hat{Y}_{in} are vacuum amplitude and phase noises, respectively, coupled into the intra-cavity field. Here, for simplicity, we do not distinguish the origin of the vacuum noises. For a complete model, please see Methods A. $G = \partial\Omega_{\text{cav}}/\partial\hat{q}$ is the optomechanical interaction strength, with Ω_{cav} the cavity angular resonance frequency; $\alpha = \sqrt{n_{\text{cav}}}$ is the classical amplitude of the intra-cavity optical field, with n_{cav} the intra-cavity photon number; m is the effective mass of the oscillator; Γ_{m} is the natural angular mechanical linewidth; and $\hat{\xi}_{\text{th}}$ is the thermal force noise.

The third term on the right-hand side of Eqn. 2 encodes the mechanical displacement \hat{q} to the optical field. Extracting this information through optical detection refines the estimation of \hat{q} , therefore decreases the uncertainty $\delta\hat{q}$ at a rate of Γ_{meas} , as shown in Fig. 1(b). Γ_{meas} is proportional to n_{cav} , η , and $1/\kappa$, with η the detection efficiency. At the same time, the second term on the right-hand side of Eq. 4 is the back-action noise, which directly couples only to the momentum quadrature at a rate of Γ_{ba} . Similarly, the thermal force noise couples directly to the momentum quadrature at a rate of $\Gamma_{\text{th}} = \Gamma_{\text{m}}n_{\text{th}}$ with n_{th} the thermal phonon occupancy of the environment. These two noises tend to increase uncertainty in $\delta\hat{p}$, as shown in Fig. 1(b). The three rates have the tendency of squeezing the mechanical state naturally. However, the quadrature rotation represented by Eq. 3 indirectly couples the back-action noise and

the thermal force noise to \hat{q} , and competes with the process of uncertainty reduction through measurement, as illustrated in Fig. 1(c). For most optomechanical systems, $\Gamma_{\text{meas}} \ll \Omega_{\text{m}}$, the quadrature rotation averages away the squeezing from measurement, leaving a circular (non-squeezed) conditional state, as shown in the upper branch of Fig. 1(c). If the measurement rate is comparable to or faster than the angular frequency of the mechanical oscillator, i.e. $\Gamma_{\text{meas}} \gtrsim \Omega_{\text{m}}$, back-action and thermal noises coupled to \hat{p} are rotated to \hat{q} slower than the reduction of $\delta\hat{q}$ by measurement, and equipartition can be violated. Thus the squeezing from measurement is preserved, as shown in the lower branch of Fig. 1(c).

The condition of $\Gamma_{\text{meas}} \gtrsim \Omega_{\text{m}}$ is easiest to achieve with low frequency mechanical oscillators. Due to excess classical noises, previous experimental efforts with low frequency mechanical oscillators were unable to achieve the preparation of quantum squeezed states, instead preparing states deemed classically squeezed, that is a state violating the equipartition between \hat{q} and \hat{p} but with no quadrature uncertainty below the ZPF [32, 33]. The previous record was set by [32], where the standard deviation of the displacement quadrature was 36 times of ZPF, i.e. 1296 times in variance.

In this work, we demonstrate the preparation of a 50 ng oscillator into a conditional mechanical classically squeezed state in post processing using casual Wiener filters for state estimation, with the lowest quadrature uncertainty in variance only (0.28 ± 0.18) dB above (1.07 ± 0.04) times the ZPF, where the uncertainty is one standard deviation of the variance. The conjugate quadrature uncertainty is (8.98 ± 0.11) dB above (7.9 ± 0.2) times of the ZPF, clearly demonstrating the violation of equipartition. This result is at the cutting edge of squeezing of the motional state of a mechanical oscillator via measurement, improving on previous record by 3 orders of magnitude. This is a significant milestone towards the quantum regime. Our work shines light on the problem of quantum-to-classical transition, especially the interplay between gravity and quantum states [6, 7, 10]. Due to the relatively large

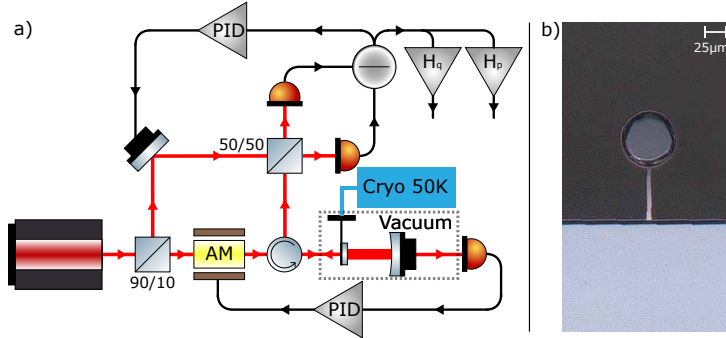


Fig. 2: (a) A simplified optical layout of the experiment. Input light is blue-detuned from the cavity resonance, stiffening the mechanical oscillator, and the system dynamics is stabilized by feeding back to the amplitude of the input light. Displacement information is readout by a balanced homodyne receiver in reflection. The photo current is saved for post processing. (b) The optomechanical resonator as imaged with a confocal laser microscope.

mass of our oscillator, it is also an ideal platform to demonstrate quantum enhanced accelerometry [34]. Because of the simple and steady control, our work also paves the way to preparing LIGO test masses into quantum squeezed states without the risk of catastrophic instability.

Experimental Setup

The optomechanical resonator used in our experiment is a high reflectivity Bragg mirror formed of 23 periods of quarter-wave optical thickness GaAs and AlGaAs. The mirror consists of a circular pad with a nominal diameter of $70 \mu\text{m}$ at the end of a nominally $55 \mu\text{m}$ long, $8 \mu\text{m}$ wide, and 220 nm thick cantilever that is attached to a ledge of the GaAs substrate. The fundamental resonance of the mirror is $\Omega_m/2\pi = 876 \text{ Hz}$ with a Q factor of 16,000 and modal mass of 50 ng . For more detail on the fabrication of the optomechanical resonator, see Refs [35–38].

The optomechanical resonator is cryogenically cooled to 50 K and has a transmissivity of 450 ppm at optical wavelength $\lambda = 1064 \text{ nm}$. This differs from the room temperature transmissivity of 250 ppm in [39] due to thermorefractive effects in the

Bragg mirror. The optomechanical resonator along with a standard highly reflecting mirror form a 1 cm long Fabry-Perot cavity that is placed under vacuum ($\sim 10^{-8}$ Torr). The cavity has a linewidth of $\kappa/2\pi = 1.77$ MHz. 79% of the input light is spatially mode-matched to the cavity, and builds up to 0.25 W of circulating power. The rest of the input light does not match the spatial mode of the cavity, and is promptly reflected. The influence of this mode mismatched part of light is considered in the model (see Methods A). The frequency of the input light is blue-detuned from the cavity resonance by a fractional detuning of $\delta_{\text{cav}} = 2\Delta/\kappa = 0.24$. Blue-detuning creates a recoil radiation pressure force on the cantilever (i.e. an optical spring), which self-locks the cavity detuning [40]. To stabilize the mechanical resonator due to the blue-detuning, we apply feedback to an amplitude modulator before the cavity using the light exiting from the 1-cm mirror, as shown in Fig. 2. The optical spring and feedback trap the mechanical oscillator at a frequency of $\Omega_{\text{eff}}/2\pi = 113.7$ kHz. Optically stiffening the mechanical oscillator in this way suppresses thermal noise [41] (see Methods F), and pushes the resonance above the frequency band where low frequency technical noises dominate.

Light exiting the cantilever is incident on a balanced homodyne receiver for phase quadrature detection. Photo current from the homodyne receiver is digitized for analysis at a 2 MHz sampling rate using a Red Pitaya STEMLab 125-14. The detection efficiency η from the cantilever to photo current is 0.42 due to losses in optics, imperfect homodyne visibility, and the quantum efficiency of the photodiodes. The cavity efficiency, intracavity power and detection chain give a high measurement rate of 61 kHz, which is 54% of the mechanical frequency, enough to violate the equipartition of energy in the displacement and momentum quadratures.

Data Analysis and the Conditional Mechanical State

The digitized homodyne photo current are saved as a time series. We fast Fourier transform the time series to get a voltage spectrum $S_{vv}[\Omega]$, which we subsequently calibrate from voltage to displacement $S_{yy}[\Omega]$ by matching the shot noise to the theoretical model (see Methods C). We then clean the calibrated spectrum by comparing it with auxiliary spectra measured at different cavity detunings (see Methods D), permitting the removal of noise common to all the spectra. As shown in Fig. 3(a), the cleaned displacement spectrum matches the model $S_{yy}[\Omega]$ well, excepting the parts influenced by non-stationary noise (e.g. to the left of the mechanical resonance). To avoid the influence of the non-stationary noise, we use the modeled $S_{yy}[\Omega]$ to compute the causal Wiener filters and to calculate the conditional state. We calculate the causal Wiener filters for displacement \hat{q} using the Wiener-Hopf Technique [26] as

$$H_q[\Omega] = \frac{1}{M_y[\Omega]} \left[\frac{S_{qy}[\Omega]}{M_y[\Omega]^*} \right]_+, \quad (5)$$

where $M_y[\Omega]$ is the causal spectral factor of $S_{yy}[\Omega]$ and $M_y[\Omega]^*$ is the anti-causal spectral factor. $M_y[\Omega]M_y[\Omega]^* = S_{yy}[\Omega]$. $[\dots]_+$ takes the causal decomposition of the function in the bracket (see Chapter 3 of [26] for details). The cross spectra $S_{qy}[\Omega]$ come from the model. $H_q[\Omega]$ is shown in Fig. 3(b).

We then apply the causal Wiener filter to S_{yy} by multiplying the two in the frequency domain to calculate the conditional displacement spectrum of the estimation error

$$S_{\delta q \delta q}[\Omega] = S_{qq}[\Omega] + |H_q[\Omega]|^2 S_{yy}[\Omega] - 2\text{Re}[H_q[\Omega] S_{qy}[\Omega]^*], \quad (6)$$

which is shown in Fig. 3(a). Similarly, we construct the Wiener filter for \hat{p} , and compute the conditional momentum spectrum $S_{\delta p \delta p}$ and cross spectrum $S_{\delta q \delta p}$ (see Methods E).

As we can see in Fig. 3(a), the conditional spectrum is strongly suppressed compared to the measured and modeled spectra. To account for the diverging displacement energy at low frequency given by the structural damping model (see Methods F and [33]), we calculate the covariances by integrating the conditional (cross) spectra from 10 kHz to 1 MHz to avoid the divergence, e.g. the cross correlation between $\delta\hat{q}$ and $\delta\hat{p}$ is $C_{\delta q\delta p} = \int_{2\pi \times 10^4 \text{ Hz}}^{2\pi \times 10^6 \text{ Hz}} \frac{d\Omega}{2\pi} \text{Re}[S_{\delta q\delta p}[\Omega]]$. Normalizing the (co)-variances to quanta in displacement $2q_{\text{zpf}}^2 = \hbar/m\Omega_{\text{eff}}$ and momentum $2p_{\text{zpf}}^2 = \hbar m\Omega_{\text{eff}}$, the covariance matrix of the estimation error is

$$\tilde{\mathbb{V}} = \begin{pmatrix} \tilde{V}_{\delta q\delta q} & \tilde{C}_{\delta q\delta p} \\ \tilde{C}_{\delta q\delta p} & \tilde{V}_{\delta p\delta p} \end{pmatrix} = \begin{pmatrix} 0.88 & 1.04 \\ 1.04 & 3.61 \end{pmatrix}, \quad (7)$$

where the tilde represents normalization to the energy quanta. The minimum eigenvalue is 0.53, only (0.28 ± 0.18) dB above (1.07 ± 0.04) times the ZPF (0.5), and the maximum eigenvalue is 3.96, (8.98 ± 0.11) dB above (7.9 ± 0.2) times the ZPF level. To properly evaluate the influence of uncertainties of experimental parameters on the conditional variances, the mean values and uncertainties reported here come from Monte Carlo uncertainty propagation. As a property of Gaussian states, the conditional covariance matrix \mathbb{V} and the mean values of the estimators $\langle \hat{q}_e \rangle$ and $\langle \hat{p}_e \rangle$ define the conditional state uniquely, and the uncertainty of the state is given by the covariance matrix. The quadrature uncertainties corresponding to \tilde{V} are shown in Fig. 3(c), with 1 standard deviation uncertainty displayed. Our result is the highest quality realization of the protocol to date, reducing the smallest variance by 3 orders of magnitude compared to the previous record [32].

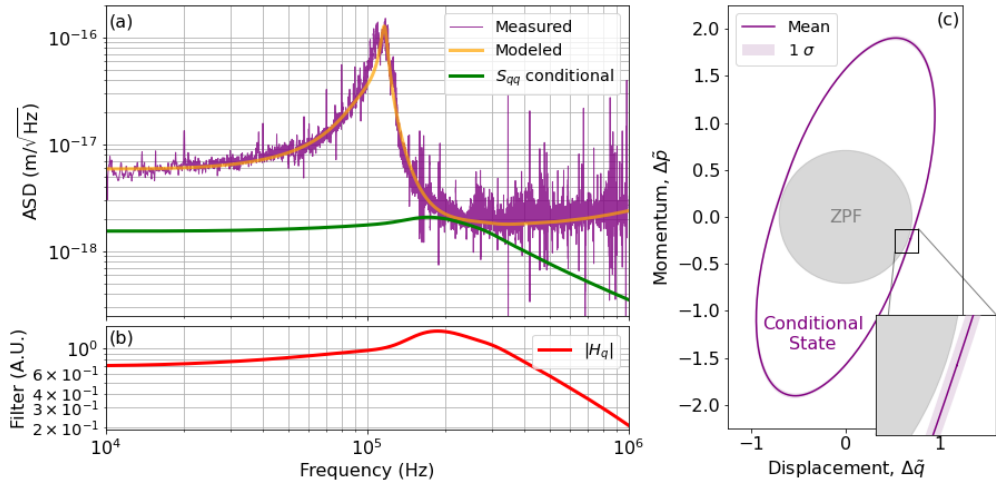


Fig. 3: a) Amplitude spectral densities of the directly measured homodyne photocurrent, the calibrated modeled homodyne photocurrent, and the displacement conditional spectrum as in Eqn. 6. b) The corresponding displacement Wiener filter as in Eqn. 5. c) Quadrature diagram of the derived conditional state. The light purple band corresponds to the region of one sigma confidence.

Discussion and Future Work

We have demonstrated preparation of a classically squeezed mechanical state approaching the quantum regime in post processing. We cleaned the measured spectrum by comparing the target spectrum to spectra taken at different cavity detunings. The same set of data compared to different auxiliary spectra shows the validity of the theoretical model. Though data cleaning is in post processing, this procedure can be converted to a real-time filter defined by the measured spectra, similar to causal Wiener filters. Together with the causal Wiener filters, real-time state preparation will be possible.

There is, however, non-stationary noise in the measurement which masks the physical motion of the mechanical oscillator and cannot be eliminated completely by data cleaning. This non-stationary noise appears in measurements at multiple positions in the experiment, and is suspected to have electronic origin. The omnipresent feature makes it challenging to hunt down and eliminate the noise. To recover the physical

displacement, we used the model to compute the causal Wiener filter and the conditional covariance matrix. This compromise prevents us from filtering the photo current to get real-time estimation of the mechanical state. Eliminating the non-stationary noises is a necessary step for quantum state preparation in real time.

Our result stands on the border line of the quantum regime. For preparation of a definitive quantum squeezed state, higher readout efficiency and lower cavity detuning (hence a lower optical spring frequency) would be helpful. The former requires optimizing the detection chain by replacing current optics with lower loss versions. The latter requires locking the optomechanical cavity on resonance, for example by using a Pound-Drever-Hall lock. Additionally, injecting light from the macroscopic mirror side of the cavity and conducting the measurement in transmission is also beneficial, as it avoids excess shot noise from the promptly reflected light that is not spatially matched to the cavity mode. With these improvements, quantum squeezed mechanical state preparation of a 50 ng mirror at room temperature should be possible [42].

Very recently, levitated particles have been prepared into quantum squeezed state in the optical regime [19]. Compared to them, our system is 7 orders of magnitude more massive. This drastic difference in mass allows our optomechanical system to explore a different region of parameter space of the classical-quantum transition, as well as to probe gravitational effects on quantized motion [10]. The steady state controls used in the continuous measurement make it straightforward to adapt these protocols to the LIGO test masses. With feedback stiffening [41] and improvements in sensitivity around 100 Hz [43], preparing the 10-kg-scale LIGO test masses in a quantum squeezed state should be possible in near future. This will be a great leap forward in studying the problem of quantum-to-classical transition. LIGO test masses will also become the most sensitive quantum enhanced accelerometers ever, which will contribute to dark matter searches [44].

Acknowledgements. We wish to thank C. Meng, W. Bowen, V. Sudhir and E. Oelker for fruitful discussions. We acknowledge the generous support from the National Science Foundation (NSF). Specifically, J.C. and B.B.L. are supported through NSF Grant No. PHY-20122088. R.E.P and S.A. are supported by NSF award PHY-2110455.

Declarations

- Conflict of interest/Competing interests: The authors declare no conflicts of interest.
- Data and code availability: Data and code underlying the results presented in this paper are not publicly available at this time but may be obtained from the authors upon request.
- Author contribution: B.B.L. and J.C. constructed the theoretical model, conducted the experiment and analyzed the data; R.E.P., S.A., X.Y. contributed to the preparation of the experiment and data taking; G.D.C. fabricated the cantilever chip; X.Y., T.R.C. and N.M. supervised the project.

Methods A Optomechanical Model

Solving the Heisenberg-Langevin equation of a single-mode cavity optomechanical system for the amplitude and phase fluctuations of the intracavity optical field (\hat{X} and \hat{Y} , respectively) and the fluctuation in the mechanical displacement \hat{q} , we have [20]

$$\begin{aligned} \hat{X}[\Omega] = & v[\Omega](\sqrt{2}G\alpha\hat{q}[\Omega] + \sqrt{\kappa_1}\hat{Y}_{\text{in}1}[\Omega] + \sqrt{\kappa_2}\hat{Y}_{\text{in}2}[\Omega] + \sqrt{\kappa_L}\hat{Y}_{\text{inL}}[\Omega]) \\ & + u[\Omega](\sqrt{\kappa_1}\hat{X}_{\text{in}1}[\Omega] + \sqrt{\kappa_2}\hat{X}_{\text{in}2}[\Omega] + \sqrt{\kappa_L}\hat{X}_{\text{inL}}[\Omega]) \end{aligned} \quad (\text{A1})$$

$$\begin{aligned} \hat{Y}[\Omega] = & u[\Omega](\sqrt{2}G\alpha\hat{q}[\Omega] + \sqrt{\kappa_1}\hat{Y}_{\text{in}1}[\Omega] + \sqrt{\kappa_2}\hat{Y}_{\text{in}2}[\Omega] + \sqrt{\kappa_L}\hat{Y}_{\text{inL}}[\Omega]) \\ & - v[\Omega](\sqrt{\kappa_1}\hat{X}_{\text{in}1}[\Omega] + \sqrt{\kappa_2}\hat{X}_{\text{in}2}[\Omega] + \sqrt{\kappa_L}\hat{X}_{\text{inL}}[\Omega]) \end{aligned} \quad (\text{A2})$$

$$\hat{q}[\Omega] = \chi_m[\Omega](\sqrt{2}\hbar G\alpha\hat{X}[\Omega] + \hat{\xi}_{\text{th}}[\Omega]), \quad (\text{A3})$$

where $G = \partial\Omega_{\text{cav}}/\partial\hat{q}$ is the optomechanical interaction strength, with Ω_{cav} the cavity angular resonance frequency; $\alpha = \sqrt{n_{\text{cav}}}$ is the classical amplitude of the intra-cavity optical field, with n_{cav} the intra-cavity photon number; κ_1 is the angular cavity coupling rate on the cantilever side, κ_2 the angular cavity loss rate on the curved mirror side, and κ_L the intra-cavity angular loss rate; $\hat{X}_{\text{in}1}$, $\hat{X}_{\text{in}2}$, and $\hat{X}_{\text{in}L}$ are the input amplitude fluctuations from the cantilever, curved mirror and internal loss; The factors $u[\Omega] = (\kappa/2 + i\Omega)/((\kappa/2 + i\Omega)^2 + \Delta^2)$, $v[\Omega] = -\Delta/((\kappa/2 + i\Omega)^2 + \Delta^2)$ are the components of the cavity susceptibility, where κ is the total angular linewidth of the cavity, and Δ the angular cavity detuning; $\hat{\xi}_{\text{th}}$ is the thermal force operator. $\chi_m[\Omega] = 1/(m(\Omega_m^2 - \Omega^2 + i\Gamma_m[\Omega]\Omega))$ is the bare mechanical susceptibility, with m , Ω_m , and $\Gamma_m[\Omega]$ the effective mass, the natural angular frequency of the mechanical mode, and the natural mechanical linewidth, respectively. Here the frequency dependence of Γ_m is a result of structural damping, which will be discussed in detail in Methods F. In most literature, the optomechanical interaction strength is rewritten in terms of $g = G\alpha x_{\text{zpf}}$, with $x_{\text{zpf}} = \sqrt{\hbar/2m\Omega_{\text{eff}}}$ the ZPF of displacement, where Ω_{eff} is the effective mechanical angular frequency influenced by optical spring and feedback. However, we intentionally keep the above form without ZPF, as Ω_{eff} is strongly influenced by optical springing in our system. Keeping G explicitly gives us an expression that works for arbitrary optical spring [45].

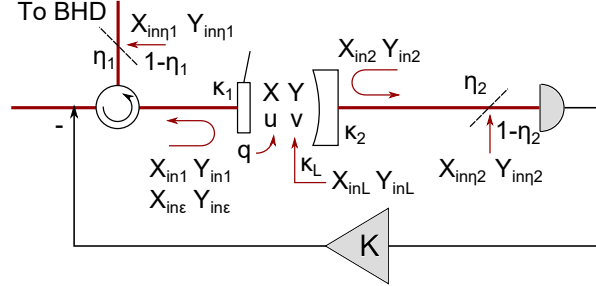


Fig. A1: The complete noise model of the experiment. Red paths represent the optical fields, and black paths electronics.

So far we have worked with an optomechanical system without feedback. In practice, as we use an optical spring to stiffen the mechanical response, feedback on the amplitude of the input laser is used to counter for the instability caused by the blue detuned laser. The feedback loop and various noise are shown in Fig. A1.

We directly detect the light exiting the curved mirror for feedback control. The open-loop representation of the amplitude fluctuation at the detector is given by

$$\hat{X}_{\text{out}2}[\Omega] = \sqrt{\eta_2}(-\hat{X}_{\text{in}2}[\Omega] + \sqrt{\kappa_2}\hat{X}[\Omega]) + \sqrt{1-\eta_2}\hat{X}_{\text{in}\eta_2}[\Omega], \quad (\text{A4})$$

where η_2 is the detection efficiency in the path, and $\hat{X}_{\text{in}\eta_2}$ the vacuum fluctuations that leaked into the signal due to imperfect detection. The transfer functions of the photo detector, feedback servo, and the amplitude modulator are wrapped up in the controller $K[\Omega]$. Then the amplitude modulated light is sent to the optomechanical cavity through the cantilever, and the intra-cavity amplitude fluctuation is given by

$$\begin{aligned} \hat{X}[\Omega] = & v[\Omega](\sqrt{2}G\alpha\hat{q}[\Omega] + \sqrt{\kappa_1}\hat{Y}_{\text{in}1}[\Omega] + \sqrt{\kappa_2}\hat{Y}_{\text{in}2}[\Omega] + \sqrt{\kappa_L}\hat{Y}_{\text{in}L}[\Omega]) \\ & + u[\Omega](\sqrt{\kappa_1}\hat{X}_{\text{in}1}[\Omega] + \sqrt{\kappa_2}\hat{X}_{\text{in}2}[\Omega] + \sqrt{\kappa_L}\hat{X}_{\text{in}L}[\Omega]) \\ & - u[\Omega]\sqrt{\kappa_1}K[\Omega](\sqrt{\eta_2}(-\hat{X}_{\text{in}2}[\Omega] + \sqrt{\kappa_2}\hat{X}[\Omega]) + \sqrt{1-\eta_2}\hat{X}_{\text{in}\eta_2}[\Omega]), \end{aligned} \quad (\text{A5})$$

where the last term is given by feedback. Collecting $\hat{X}[\Omega]$ on both sides, we get the close-loop expression of $\hat{X}[\Omega]$:

$$\begin{aligned} \hat{X}[\Omega] = & \frac{1}{1 + \sqrt{\eta_2\kappa_1\kappa_2}K[\Omega]u[\Omega]} (v[\Omega](\sqrt{2}G\alpha\hat{q}[\Omega] + \sqrt{\kappa_1}\hat{Y}_{\text{in}1}[\Omega] + \sqrt{\kappa_2}\hat{Y}_{\text{in}2}[\Omega] + \sqrt{\kappa_L}\hat{Y}_{\text{in}L}[\Omega]) \\ & + u[\Omega](\sqrt{\kappa_1}\hat{X}_{\text{in}1}[\Omega] + \sqrt{\kappa_2}\hat{X}_{\text{in}2}[\Omega] + \sqrt{\kappa_L}\hat{X}_{\text{in}L}[\Omega]) \\ & + u[\Omega]\sqrt{\kappa_1}K[\Omega](\sqrt{\eta_2}\hat{X}_{\text{in}2}[\Omega] - \sqrt{1-\eta_2}\hat{X}_{\text{in}\eta_2}[\Omega])). \end{aligned} \quad (\text{A6})$$

Similarly, the close-loop $\hat{Y}[\Omega]$ is

$$\begin{aligned}\hat{Y}[\Omega] = & u[\Omega](\sqrt{2}G\alpha\hat{q}[\Omega] + \sqrt{\kappa_1}\hat{Y}_{\text{in}1}[\Omega] + \sqrt{\kappa_2}\hat{Y}_{\text{in}2}[\Omega] + \sqrt{\kappa_L}\hat{Y}_{\text{in}L}[\Omega]) \\ & - v[\Omega](\sqrt{\kappa_1}\hat{X}_{\text{in}1}[\Omega] + \sqrt{\kappa_2}\hat{X}_{\text{in}2}[\Omega] + \sqrt{\kappa_L}\hat{X}_{\text{in}L}[\Omega]) \\ & + v[\Omega]\sqrt{\kappa_1}K[\Omega](\sqrt{\eta_2}(-\hat{X}_{\text{in}2}[\Omega] + \sqrt{\kappa_2}\hat{X}[\Omega]) + \sqrt{1-\eta_2}\hat{X}_{\text{in}\eta_2}[\Omega]),\end{aligned}\quad (\text{A7})$$

where we have kept the compact form of $\hat{X}[\Omega]$ in the last line for simplicity. Plugging Eq. A6 into Eq. A3, and collecting $\hat{q}[\Omega]$, we can see the mechanical susceptibility is modified to be

$$\chi_{\text{eff}}[\Omega] = \left(\chi_{\text{m}}^{-1}[\Omega] - \frac{2\hbar G^2 n_{\text{cav}} v[\Omega]}{1 + \sqrt{\eta_2 \kappa_1 \kappa_2} K[\Omega] u[\Omega]} \right)^{-1}. \quad (\text{A8})$$

The second term in the parenthesis includes the effects of the optical spring in the numerator and feedback in the denominator.

Now we consider the optical field being sent to the balanced homodyne detector (BHD). The input-output relation of a cavity gives an expression of the mode-matched part of the field reflecting off the cantilever $-\hat{X}_{\text{in}1}[\Omega] + \sqrt{\kappa_1}\hat{X}[\Omega]$ for amplitude and $-\hat{Y}_{\text{in}1}[\Omega] + \sqrt{\kappa_1}\hat{Y}[\Omega]$ for phase. Due to the non-ideal mode matching of the input laser to the cavity, we have promptly reflected optical field that corresponds to higher order modes of the cavity. This field is also amplitude modulated by the feedback, and is given by

$$\hat{X}_{\text{infb}\epsilon}[\Omega] = K[\Omega](\sqrt{\eta_2}(-\hat{X}_{\text{in}2}[\Omega] + \sqrt{\kappa_2}\hat{X}[\Omega]) + \sqrt{1-\eta_2}\hat{X}_{\text{in}\eta_2}[\Omega]) + \hat{X}_{\text{in}\epsilon}[\Omega], \quad (\text{A9})$$

where $\hat{X}_{\text{in}\epsilon}[\Omega]$ is the vacuum fluctuation of this field. The phase quadrature is simply $\hat{Y}_{\text{in}\epsilon}[\Omega]$. Writing the mode match as ϵ , we have the output amplitude and phase

quadratures as

$$\begin{aligned}\hat{X}_{\text{out}1}[\Omega] = & \sqrt{\eta_1} \left(-e^{i\phi} \sqrt{1-\epsilon} \hat{X}_{\text{inf}\epsilon}[\Omega] + \sqrt{\epsilon} (-\hat{X}_{\text{in}1}[\Omega] + \sqrt{\kappa_1} \hat{X}[\Omega]) \right) \\ & + \sqrt{1-\eta_1} \hat{X}_{\text{in}\eta_1}[\Omega]\end{aligned}\quad (\text{A10})$$

$$\begin{aligned}\hat{Y}_{\text{out}1}[\Omega] = & \sqrt{\eta_1} \left(-e^{i\phi} \sqrt{1-\epsilon} \hat{Y}_{\text{in}\epsilon}[\Omega] + \sqrt{\epsilon} (-\hat{Y}_{\text{in}1}[\Omega] + \sqrt{\kappa_1} \hat{Y}[\Omega]) \right) \\ & + \sqrt{1-\eta_1} \hat{Y}_{\text{in}\eta_1}[\Omega],\end{aligned}\quad (\text{A11})$$

where η_1 is the detection efficiency, ϕ the effective Gouy phase difference between the mode-mismatched field and the mode-matched one, and $\hat{X}_{\text{in}\eta_1}[\Omega]$ and $\hat{Y}_{\text{in}\eta_1}[\Omega]$ the vacuum fluctuations due to loss. At the BHD, the detected field is given by

$$\hat{X}_{\text{out}1}^\theta[\Omega] = \hat{X}_{\text{out}1}[\Omega] \cos(\theta) + \hat{Y}_{\text{out}1}[\Omega] \sin(\theta), \quad (\text{A12})$$

with θ the homodyne angle.

As $\hat{X}_{\text{out}1}[\Omega]$ and $\hat{Y}_{\text{out}1}[\Omega]$ are linear functions of $\hat{q}[\Omega]$, we can write the detected field in displacement unit by dividing both sides of Eq. A12 by the pre-factor of \hat{q} to get

$$\hat{y}[\Omega] = \hat{q}[\Omega] + \hat{z}[\Omega], \quad (\text{A13})$$

where \hat{z} is the imprecision noise in displacement unit. \hat{y} is sometimes referred as the apparent displacement.

Methods B Optical Parameter Characterization

Accurate characterization of optical parameters such as cavity linewidth, cavity detuning, and intracavity power is crucial for constructing the theoretical model of the

experiment. Here, we introduce our method to determine these parameters within 3% uncertainty.

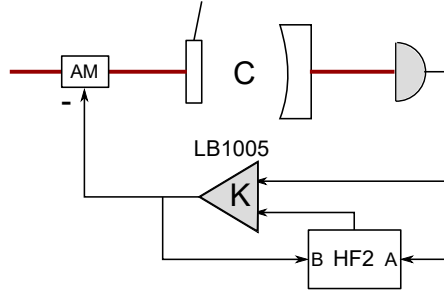


Fig. B2: Open-loop cavity transfer function measurement scheme. C and K stand for the transfer functions of the cavity and the control servo (LB1005) respectively. HF2 works as a vector network analyzer. AM stands for the amplitude modulator used to stabilize the cavity.

We use the optical spring to constrain the optical parameters, as in [36]. The optical spring frequency is determined by measuring the open-loop cavity transfer function from amplitude fluctuations to photo current. The measurement scheme is shown in Fig. B2. A Newport LB1005 servo is used to lock the cavity, and as a sum point of signal and drive. A Zürich Instrument HF2 lock-in amplifier is used as the vector network analyzer. The signals right before and after the servo are fed to the two inputs A and B of the HF2, where the ratio of the two is computed. The transfer function of the amplitude modulator is flat in the frequency range we are interested in. Therefore, it only contributes a constant factor to the loop, which is absorbed to the controller K for simplicity. The close-loop inputs to Port A and B of the HF2 are given by

$$A = \frac{CK}{1 + CK}d \quad (\text{B14})$$

$$B = \frac{K}{1 + CK}d, \quad (\text{B15})$$

where d is the drive, and C the open-loop transfer function of the cavity. Taking the ratio A/B , we can recover the desired transfer function C .

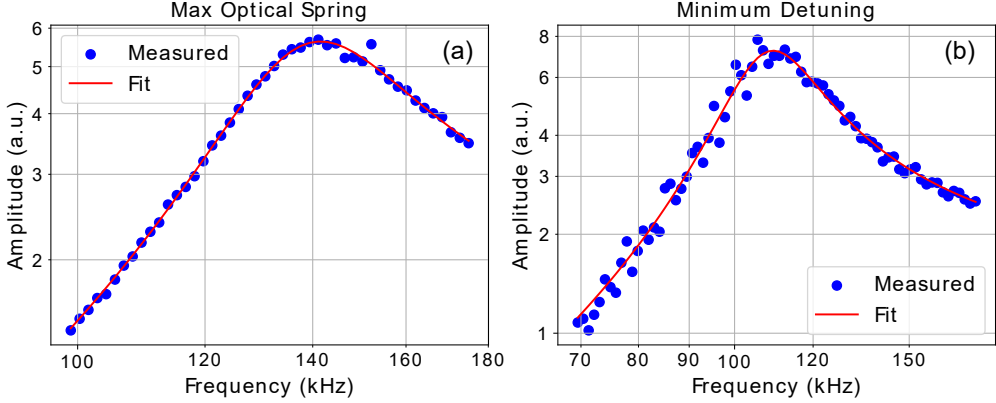


Fig. B3: Amplitudes of open-loop cavity transfer functions for (a) maximum optical spring frequency, and (b) minimum cavity detuning.

Firstly, we lock the cavity on the blue detuning side, and change the cavity length to find the transfer function with maximum optical spring frequency. The result is shown in Fig. B3(a). In the bad-cavity regime ($\kappa \gg \Omega_{\text{eff}}$), this corresponds to a fractional detuning of $\delta_{\text{cav}} = 1/\sqrt{3}$. We fix the detuning and fit the intracavity power and total cavity linewidth. The fitting uncertainties of both parameters are below 2%.

Secondly, we hold the input power constant, and change cavity length to minimize the detuning. As for fitting, we fix the intracavity optical power, which is computed by comparing DC voltages at the photo detector in the maximum optical spring frequency case and the minimum detuning case. The intracavity loss is known to change with intracavity power, as a result of radiation pressure changing the alignment of the cavity [36]. We let the detuning and cavity linewidth to be free parameters. The measured transfer function and fitting is shown in Fig. B3(b), and the fitting uncertainties of the parameters are below 3%. As our cavity locking scheme relies on the slope of the cavity resonance, the lowest fractional detuning we can achieve is $\delta_{\text{cav}} = 0.24$.

As the transfer functions of the servo, amplitude modulator and photo detector are essential for the theoretical model, we also measure them separately using the HF2, and input the results to our model.

Table B1: Key experimental parameters

$\kappa/2\pi$	1.77 MHz	Ω_m	876 Hz
δ_{cav}	0.24	Q factor	16000
P_{cav}	0.25 W	Ω_{eff}	113.7 Hz
η	0.42	T	50 K
λ	1064 nm	m	50 ng

Methods C Calibration

The homodyne photo current power spectrum is measured in units of V^2/Hz . As the theoretical model is in terms of the cantilever displacement power spectrum with units of m^2/Hz , we must calibrate our measured spectrum. At small displacements, the cantilever motion induces a linear phase shift on the light reflected from the cavity. The reflected light is then measured using a homodyne detector that is operated within the linear regime, leading to a linear relationship between the measured photocurrent and the cantilever displacement power spectra.

To determine the calibration factor, we align the shot noise dominated regime above 300kHz. As there are narrow regions of excess noise in the raw data, we create a histogram of measured amplitude spectral density (ASD) values as can be seen in Fig. C4 and use the peak of the distribution for the calibration. With a modeled shot noise of $1.7341e-18 m/\sqrt{Hz}$ and a measured shot noise of $2.1951e-6 V/\sqrt{Hz}$, the calibration factor is $7.9e-13 m/V$.

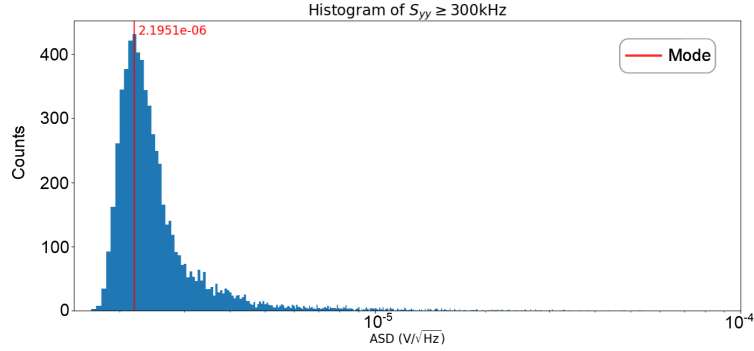


Fig. C4: Histogram of the measured homodyne photocurrent amplitude spectral density in the shot noise dominated regime above 300 kHz. The mode of the distribution occurs at an ASD of 2.1951×10^{-6} . This is used to calculate the calibration of the raw data from Volts to meters in the presence of excess noise.

Methods D Noisy Background Cancellation

The direct spectra of the homodyne photo currents contain noises not included in the theoretical model, such as classical laser phase noise, higher order mechanical modes of the cantilever, mechanical motion of the structure holding the optomechanical cavity, noise from the piezo used to lock the cavity, calibration tones etc. Here we introduce a noise cancellation procedure to recover the spectrum of the fundamental mechanical mode and quantum shot noise from the noisy environment. The basic idea is to use homodyne spectra measured with different experimental parameters, especially different cavity detunings, to eliminate the stationary excess noises in the target spectrum. In the following, we refer the spectra used to clean the target spectrum as auxiliary spectra.

As the whole system is linear, the entire experimental apparatus from the optomechanical cavity to the homodyne receiver can be treated as a transfer function from various noises to homodyne photo current. There are two types of input noises — force and phase noises. Examples of force noises, which drive actual motion of the mechanical oscillator, include thermal force noise and laser amplitude noise like quantum back-action. Phase noises appear as apparent motion due to the sensing apparatus,

such as quantum shot noise and classical laser phase noise. We indicate force noise included in the model as f_{mod} and force noise not included as f_{non} . Similarly, we indicate the corresponding phase noises as ϕ_{mod} and ϕ_{non} for modeled and unmodeled noises respectively. For illustration purpose, we suppose the homodyne receiver detects the intra-cavity phase quadrature. Then the force noises are transferred to phase noises through a transfer function TF_f , which is a result of the mechanical susceptibility and the cavity optomechanical interaction. Moreover, the cavity and the homodyne transfer phase noise input to photo current through TF_ϕ . We can write the photo current of any measurement as

$$((f_{\text{mod}} + f_{\text{non}})\text{TF}_f + \phi_{\text{mod}} + \phi_{\text{non}})\text{TF}_\phi, \quad (\text{D16})$$

and the corresponding spectrum as

$$S_{\text{meas}} = |((f_{\text{mod}} + f_{\text{non}})\text{TF}_f + \phi_{\text{mod}} + \phi_{\text{non}})\text{TF}_\phi|^2. \quad (\text{D17})$$

The modeled spectrum in the same case is

$$S_{\text{mod}} = |(f_{\text{mod}}\text{TF}_f + \phi_{\text{mod}})\text{TF}_\phi|^2. \quad (\text{D18})$$

Now we consider the auxiliary spectra, formally the same as the expressions above, but with transfer functions and spectra labelled by superscripts “aux”. Taking the ratio between $S_{\text{meas}}^{\text{aux}}$ and $S_{\text{mod}}^{\text{aux}}$, we can eliminate the transfer function $\text{TF}_\phi^{\text{aux}}$, i.e. the excess noises do not influence how phase noises are transferred into photo currents:

$$\frac{S_{\text{meas}}^{\text{aux}}}{S_{\text{mod}}^{\text{aux}}} = \frac{|(f_{\text{mod}} + f_{\text{non}})\text{TF}_f^{\text{aux}} + \phi_{\text{mod}} + \phi_{\text{non}}|^2}{|f_{\text{mod}}\text{TF}_f^{\text{aux}} + \phi_{\text{mod}}|^2}. \quad (\text{D19})$$

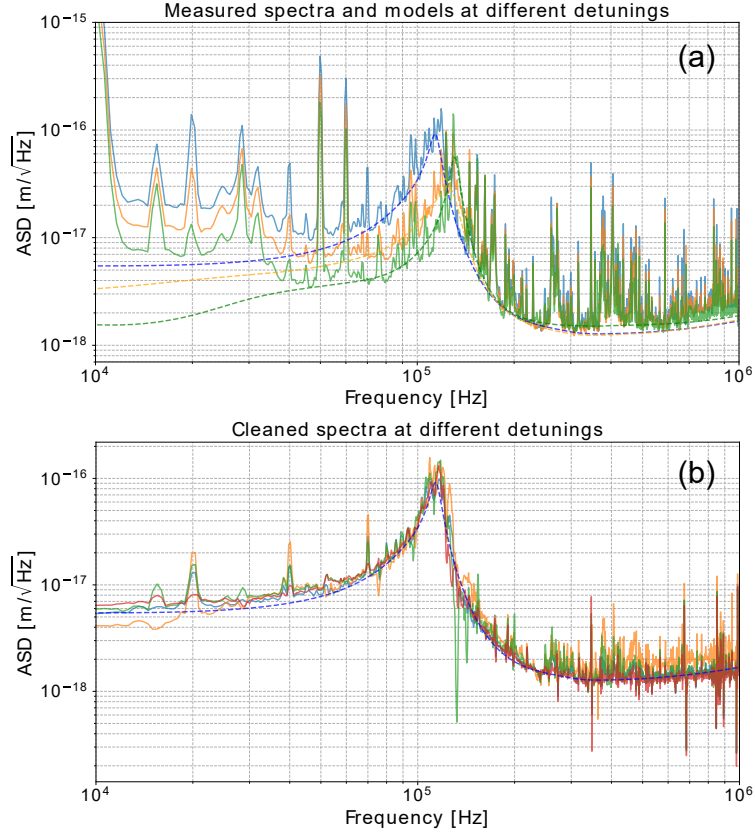


Fig. D5: (a) Examples of spectra of homodyne photo currents (calibrated to displacement unit) at different detunings (solid lines) against the corresponding modelled spectra (dashed lines). Blue, orange and green curves correspond to the lowest, intermediate and the highest detuning used in the measurement respectively. (b) Cleaned spectra of the lowest detuning measurement using 4 different auxiliary measurements. The solid curves are the cleaned data, and the dashed curve is the model.

For stationary noises, this ratio gives the fraction of the modelled noise to the total noise.

Now consider the target noisy measured spectrum S_{meas}^t labelled by superscripts “t”, which is taken with the optimal experimental parameters for mechanical squeezing (with transfer functions TF_f^t and TF_ϕ^t), and the same input noise, i.e. under the assumption that the noises are stationary between measurements. We can clean the

spectrum by dividing S_{meas}^t by the ratio $S_{\text{meas}}^{\text{aux}}/S_{\text{mod}}^{\text{aux}}$:

$$S_{\text{clean}} = \frac{S_{\text{mod}}^{\text{aux}} S_{\text{meas}}^t}{S_{\text{meas}}^{\text{aux}}} \quad (\text{D20})$$

$$= \frac{|f_{\text{mod}} \text{TF}_f^{\text{aux}} + \phi_{\text{mod}}|^2 |(f_{\text{mod}} + f_{\text{non}}) \text{TF}_f^t + \phi_{\text{mod}} + \phi_{\text{non}}|^2 |\text{TF}_\phi^t|^2}{|(f_{\text{mod}} + f_{\text{non}}) \text{TF}_f^{\text{aux}} + \phi_{\text{mod}} + \phi_{\text{non}}|^2}. \quad (\text{D21})$$

Now we evaluate this cleaned data in two regimes: the mechanical motion dominated regime (around and below the stiffened mechanical resonance frequency) and the phase noise dominated regime (at high frequencies). In the mechanical motion dominated regime $\phi_{\text{mod}}, \phi_{\text{non}} \rightarrow 0$, we can rewrite the cleaned spectrum as

$$S_{\text{clean}} \approx \frac{|f_{\text{mod}} \text{TF}_f^{\text{aux}}|^2 |(f_{\text{mod}} + f_{\text{non}}) \text{TF}_f^t|^2 |\text{TF}_\phi^t|^2}{|(f_{\text{mod}} + f_{\text{non}}) \text{TF}_f^{\text{aux}}|^2} = |f_{\text{mod}} \text{TF}_f^t|^2 |\text{TF}_\phi^t|^2 \quad (\text{D22})$$

$$\approx S_{\text{mod}}^t = |(f_{\text{mod}} \text{TF}_f^t + \phi_{\text{mod}}) \text{TF}_\phi^t|^2, \quad (\text{D23})$$

where the modeled spectrum for the target measurement S_{mod}^t inherits the form of Eq. D18. In the phase noise dominated regime $f_{\text{mod}}, f_{\text{non}} \rightarrow 0$, we have

$$S_{\text{clean}} \approx \frac{|\phi_{\text{mod}}|^2 |\phi_{\text{mod}} + \phi_{\text{non}}|^2 |\text{TF}_\phi^t|^2}{|\phi_{\text{mod}} + \phi_{\text{non}}|^2} = |\phi_{\text{mod}}|^2 |\text{TF}_\phi^t|^2 \approx S_{\text{mod}}^t. \quad (\text{D24})$$

Therefore, in both regimes, the cleaned data recovers the modeled spectrum (i.e. the mechanical motion of the fundamental mode and quantum shot noise) and cleans up the excess noises. In general, the cleaned data does not recover the model in the intermediate regime, appearing at the frequencies where the tail of the mechanical peak and the shot noise meet. However, experimental data in this regime is covered by loud laser phase noise, making it phase noise dominated again. Thus, the data cleaning procedure recovers the motion of the desired mechanical mode and the shot noise from the entire noisy spectrum.

Figure D5 illustrates our noise cancellation procedure. We took homodyne photo currents for different cavity detunings, the sample spectra of which are shown in Fig. D5(a). The sharp peaks at low frequencies aligning with integer number of 10 kHz are the piezo calibration tone at 10 kHz and its harmonics. At 60 kHz a phase calibration tone overlaps with harmonics of the piezo calibration tone. At non-integer 10 kHz frequencies, the sharp peaks are high order mechanical modes, which couple weakly to the cavity field, and do not experience significant optical springing. The broad structure around 28 kHz corresponds to the cavity piezo resonance. The common sharp structures above 130 kHz are phase noises from the laser and fibers. Figure D5(b) shows the spectra of the lowest detuning measurement cleaned by 4 different auxiliary spectra. All spectra match the modelled curve well. We notice that around the optical springed mechanical resonance, there are some noise peaks that are not consistent among the spectra. These structures correspond to non-stationary electronic noise. The harmonics of the piezo calibration tone are mitigated in the cleaned spectra, but not eliminated, as the nonlinearity of the piezo response depends on the DC bias, which can differ from measurement to measurement. Due to these non-stationary noises, we calculate the final mechanical squeezing using the model instead of the cleaned data.

Methods E Momentum and cross spectra of the fundamental mechanical mode

In Fig. 3 of the main text, we only show the displacement related spectra and causal Wiener filter. Here we show the momentum related spectra and filter in Fig. E6 for the purpose of completeness. The momentum and displacement spectra are related by $S_{pp}[\Omega] = m^2\Omega^2 S_{qq}[\Omega]$, which is true for both \hat{q} , \hat{p} and $\delta\hat{q}$, $\delta\hat{p}$. As a result, the momentum spectrum is suppressed at low frequencies, while enhanced at higher frequencies.

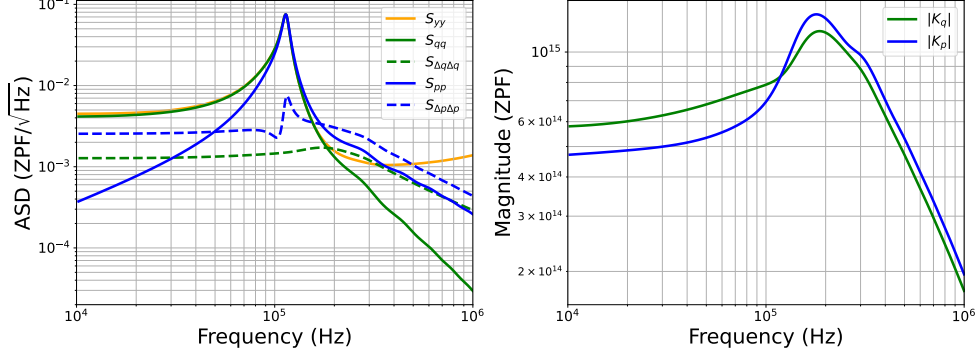


Fig. E6: **Left panel:** ASDs of spectra normalized to ZPF. **Right panel:** Magnitudes of causal Wiener filters for \hat{q} and \hat{p} normalized to ZPF.

As for the conditional momentum and cross spectra, we construct the causal Wiener filter for \hat{p} similar to $H_q(\Omega)$ as

$$H_p[\Omega] = \frac{1}{M_y[\Omega]} \left[\frac{S_{py}[\Omega]}{M_y[\Omega]^*} \right]_+, \quad (\text{E25})$$

where S_{py} comes from the model. Then the conditional spectra are given by

$$S_{\delta p \delta p}[\Omega] = S_{pp}[\Omega] + |H_p[\Omega]|^2 S_{yy}[\Omega] - 2\text{Re}[H_p[\Omega] S_{py}[\Omega]^*] \quad (\text{E26})$$

$$S_{\delta q \delta p}[\Omega] = S_{qp}[\Omega] + H_q[\Omega] H_p[\Omega]^* S_{yy}[\Omega] - H_p[\Omega]^* S_{qy}[\Omega] - H_q[\Omega] S_{py}[\Omega]^* \quad (\text{E27})$$

for momentum and cross spectra respectively.

Methods F Structural Damping and Choice of Integration Band

Structural damping is typically the dominant loss channel for mechanical structures in high vacuum [41, 46–49]. The most common model for structural damping is

characterized by a constant loss angle ϕ_1 , which results in the mechanical susceptibility

$$\chi_m[\Omega] = \frac{1}{m(\Omega_m^2 - \Omega^2 + i\Omega_m^2\phi_1)} = \frac{1}{m(\Omega_m^2 - \Omega^2 + i\Gamma_m[\Omega]\Omega)}, \quad (\text{F28})$$

where $\Gamma_m[\Omega] = \Omega_m^2\phi_1/\Omega$ has a $1/\Omega$ dependence. This implies that employing an optical spring to increase the mechanical resonance frequency can improve the thermal coherence of the oscillator [41]. The fluctuation-dissipation theorem gives the thermal displacement spectrum [50, 51]

$$\begin{aligned} S_{qq}^{\text{th}}[\Omega] &= -4\hbar \left(n_{\text{th}}[\Omega] + \frac{1}{2} \right) \text{Im}[\chi_m[\Omega]] \\ &= \frac{4\hbar(n_{\text{th}}[\Omega] + \frac{1}{2})}{m((\Omega^2 - \Omega_m^2) + (\Omega_m\phi_1)^2)}, \end{aligned} \quad (\text{F29})$$

with $n_{\text{th}}[\Omega] = 1/(\exp[\hbar\Omega/k_B T] - 1)$ being the thermal occupancy of the bath, where k_B is the Boltzmann constant, and T the bath temperature. The factor of 4 in front of \hbar is due to the single-side spectrum. In the high temperature limit, $n_{\text{th}} \approx k_B T/\hbar\Omega$, which gives $S_{qq}^{\text{th}}[\Omega]$ a $1/\Omega$ dependence. The thermal noise of our cantilever mode reproduces this feature [36] as expected.

However, this model is unphysical. The thermal displacement spectrum diverges at low frequency, which leads to infinite energy and hinders proper state estimation. Moreover, the requirement of real time domain susceptibility $\chi_m(t)$ calls for $\phi_1[\Omega]$ to be an odd function [29, 52]. A non-zero constant value of ϕ_1 certainly violates this rule.

To avoid this issue, the authors of [33] introduced a roll-off frequency to give ϕ_1 a frequency dependence while keep $\int_0^{+\infty} \frac{d\Omega}{2\pi} S_{qq}^{\text{th}}[\Omega] = (2n_{\text{th}} + 1)V_{\text{qzpf}}$, i.e. preserve equipartition of thermal noise. Alternatively, a Zener model type loss angle can be used instead of a constant ϕ_1 [29, 53]. Practically, either of the methods is equivalent to introducing a cut off frequency Ω_1 to the lower end of the integration band. In addition,

we can also introduce a cut off frequency Ω_h to the higher end for computational convenience.

We choose cut off frequencies that preserves equipartition of thermal noises, as in [33]. However, as the optical spring and feedback shift the mechanical frequency by 2 orders of magnitude, using the natural frequency and linewidth to calculate thermal noise is not a physical choice. Instead, we model a mechanical oscillator coupled to the same thermal bath as our real oscillator with susceptibility

$$\chi_m[\Omega] = \frac{1}{m(\Omega_{\text{eff}}^2 - \Omega^2 + i\Omega_{\text{eff}}^2 \phi_1)}, \quad (\text{F30})$$

where Ω_{eff} is the resonance frequency of the real fundamental mode after optical spring and feedback, and ϕ_1 is kept constant. Applying the fluctuation dissipation theorem, we can compute $S_{\text{qq}}^{\text{th}}$. Using the relation $S_{\text{pp}}^{\text{th}}[\Omega] = m^2 \Omega^2 S_{\text{qq}}^{\text{th}}[\Omega]$, we get the spectrum of momentum. Then we compute variances normalized to phonon number as

$$V_{\text{oo}}^{\text{th}} = \int_{\Omega_1}^{\Omega_h} \frac{d\Omega}{2\pi} \frac{S_{\text{oo}}^{\text{th}}[\Omega]}{2V_{\text{ozpf}}}, \quad (\text{F31})$$

where $\hat{o} = \hat{q}$ or \hat{p} , and the zero-point variance is computed using Ω_{eff} . We choose Ω_h to be as large as possible. As we change Ω_1 from 10 Hz to 50 kHz, the difference $V_{\text{qq}}^{\text{th}}/V_{\text{pp}}^{\text{th}} - 1$ changes from 3^{-4} to 2^{-5} . This indicates that the state estimation should be insensitive to the choice of the lower cut off frequency. In practice, we choose $\Omega_1/(2\pi) = 10$ kHz, and $\Omega_h/(2\pi) = 1$ MHz for squeezing computation.

References

- [1] Hollenhorst, J.N.: Quantum limits on resonant-mass gravitational-radiation detectors. *Physical Review D* **19**(6), 1669 (1979)
- [2] Aspelmeyer, M., Kippenberg, T.J., Marquardt, F.: Cavity optomechanics. *Rev.*

- Mod. Phys. **86**, 1391–1452 (2014) <https://doi.org/10.1103/RevModPhys.86.1391>
- [3] Lo, H.-Y., Kienzler, D., Clercq, L., Marinelli, M., Negnevitsky, V., Keitch, B.C., Home, J.P.: Spin–motion entanglement and state diagnosis with squeezed oscillator wavepackets. *Nature* **521**(7552), 336–339 (2015)
- [4] Schlegel, D.S., Minganti, F., Savona, V.: Quantum error correction using squeezed schrödinger cat states. *Phys. Rev. A* **106**, 022431 (2022) <https://doi.org/10.1103/PhysRevA.106.022431>
- [5] Hillmann, T., Quijandría, F.: Quantum error correction with dissipatively stabilized squeezed-cat qubits. *Phys. Rev. A* **107**, 032423 (2023) <https://doi.org/10.1103/PhysRevA.107.032423>
- [6] Diósi, L.: Gravitation and quantum-mechanical localization of macro-objects. *Physics Letters A* **105**(4), 199–202 (1984) [https://doi.org/10.1016/0375-9601\(84\)90397-9](https://doi.org/10.1016/0375-9601(84)90397-9)
- [7] Penrose, R.: On gravity’s role in quantum state reduction. *General relativity and gravitation* **28**, 581–600 (1996)
- [8] Bassi, A., Ghirardi, G.: Dynamical reduction models. *Physics Reports* **379**(5), 257–426 (2003) [https://doi.org/10.1016/S0370-1573\(03\)00103-0](https://doi.org/10.1016/S0370-1573(03)00103-0)
- [9] Chen, Y.: Macroscopic quantum mechanics: theory and experimental concepts of optomechanics. *Journal of Physics B: Atomic, Molecular and Optical Physics* **46**(10), 104001 (2013)
- [10] Lami, L., Pedernales, J.S., Plenio, M.B.: Testing the quantumness of gravity without entanglement. *Phys. Rev. X* **14**, 021022 (2024) <https://doi.org/10.1103/PhysRevX.14.021022>

- [11] Wollman, E.E., Lei, C., Weinstein, A., Suh, J., Kronwald, A., Marquardt, F., Clerk, A.A., Schwab, K.: Quantum squeezing of motion in a mechanical resonator. *Science* **349**(6251), 952–955 (2015)
- [12] Pirkkalainen, J.-M., Damskäg, E., Brandt, M., Massel, F., Sillanpää, M.A.: Squeezing of quantum noise of motion in a micromechanical resonator. *Physical Review Letters* **115**(24), 243601 (2015)
- [13] Lecocq, F., Clark, J.B., Simmonds, R.W., Aumentado, J., Teufel, J.D.: Quantum nondemolition measurement of a nonclassical state of a massive object. *Physical Review X* **5**(4), 041037 (2015)
- [14] Lei, C.U., Weinstein, A.J., Suh, J., Wollman, E.E., Kronwald, A., Marquardt, F., Clerk, A.A., Schwab, K.C.: Quantum nondemolition measurement of a quantum squeezed state beyond the 3 db limit. *Phys. Rev. Lett.* **117**, 100801 (2016) <https://doi.org/10.1103/PhysRevLett.117.100801>
- [15] Ma, X., Viennot, J.J., Kotler, S., Teufel, J.D., Lehnert, K.W.: Non-classical energy squeezing of a macroscopic mechanical oscillator. *Nature Physics* **17**(3), 322–326 (2021)
- [16] Marti, S., Lüpke, U., Joshi, O., Yang, Y., Bild, M., Omahen, A., Chu, Y., Fadel, M.: Quantum squeezing in a nonlinear mechanical oscillator. *Nature Physics*, 1–6 (2024)
- [17] Shomroni, I., Qiu, L., Malz, D., Nunnenkamp, A., Kippenberg, T.J.: Optical backaction-evading measurement of a mechanical oscillator. *Nature communications* **10**(1), 2086 (2019)
- [18] Xin, M., Leong, W.S., Chen, Z., Wang, Y., Lan, S.-Y.: Rapid quantum squeezing by jumping the harmonic oscillator frequency. *Phys. Rev. Lett.* **127**, 183602

- (2021) <https://doi.org/10.1103/PhysRevLett.127.183602>
- [19] Rossi, M., Militaru, A., Zambon, N.C., Riera-Campenya, A., Romero-Isart, O., Frimmer, M., Novotny, L.: Quantum delocalization of a levitated nanoparticle. arXiv preprint arXiv:2408.01264 (2024)
- [20] Rossi, M., Mason, D., Chen, J., Tsaturyan, Y., Schliesser, A.: Measurement-based quantum control of mechanical motion. *Nature* **563**(7729), 53–58 (2018)
- [21] Tebbenjohanns, F., Mattana, M.L., Rossi, M., Frimmer, M., Novotny, L.: Quantum control of a nanoparticle optically levitated in cryogenic free space. *Nature* **595**(7867), 378–382 (2021)
- [22] Magrini, L., Rosenzweig, P., Bach, C., Deutschmann-Olek, A., Hofer, S.G., Hong, S., Kiesel, N., Kugi, A., Aspelmeyer, M.: Real-time optimal quantum control of mechanical motion at room temperature. *Nature* **595**(7867), 373–377 (2021)
- [23] Doherty, A.C., Jacobs, K.: Feedback control of quantum systems using continuous state estimation. *Phys. Rev. A* **60**, 2700–2711 (1999) <https://doi.org/10.1103/PhysRevA.60.2700>
- [24] Müller-Ebhardt, H., Rehbein, H., Li, C., Mino, Y., Somiya, K., Schnabel, R., Danzmann, K., Chen, Y.: Quantum-state preparation and macroscopic entanglement in gravitational-wave detectors. *Phys. Rev. A* **80**, 043802 (2009) <https://doi.org/10.1103/PhysRevA.80.043802>
- [25] Meng, C., Brawley, G.A., Bennett, J.S., Vanner, M.R., Bowen, W.P.: Mechanical squeezing via fast continuous measurement. *Phys. Rev. Lett.* **125**, 043604 (2020) <https://doi.org/10.1103/PhysRevLett.125.043604>
- [26] Kailath, T.: Lectures on Wiener and Kalman Filtering. Springer (1981). <https://doi.org/10.1007/978-1-4613-9770-1>

[//link.springer.com/book/10.1007/978-3-7091-2804-6](https://link.springer.com/book/10.1007/978-3-7091-2804-6)

- [27] Wieczorek, W., Hofer, S.G., Hoelscher-Obermaier, J., Riedinger, R., Hammerer, K., Aspelmeyer, M.: Optimal state estimation for cavity optomechanical systems. *Phys. Rev. Lett.* **114**, 223601 (2015) <https://doi.org/10.1103/PhysRevLett.114.223601>
- [28] Rossi, M., Mason, D., Chen, J., Schliesser, A.: Observing and verifying the quantum trajectory of a mechanical resonator. *Phys. Rev. Lett.* **123**, 163601 (2019) <https://doi.org/10.1103/PhysRevLett.123.163601>
- [29] Chen, J., Lane, B.B., Direkci, S., Ganapathy, D., Yin, X., Mavalvala, N., Chen, Y., Sudhir, V.: Causal state estimation and the heisenberg uncertainty principle. *Phys. Rev. A* **110**, 022207 (2024) <https://doi.org/10.1103/PhysRevA.110.022207>
- [30] Bouten, L., Handel, R.V.: On the Separation Principle in Quantum Control, pp. 206–238. World Scientific (2008). https://doi.org/10.1142/9789812832962_0010
- [31] Doherty, A.C., Tan, S.M., Parkins, A.S., Walls, D.F.: State determination in continuous measurement. *Phys. Rev. A* **60**, 2380–2392 (1999) <https://doi.org/10.1103/PhysRevA.60.2380>
- [32] Santiago-Condori, J.G., Yamamoto, N., Matsumoto, N.: Verification of conditional mechanical squeezing for a mg-scale pendulum near quantum regimes. arXiv preprint arXiv:2008.10848 (2020)
- [33] Meng, C., Brawley, G.A., Khademi, S., Bridge, E.M., Bennett, J.S., Bowen, W.P.: Measurement-based preparation of multimode mechanical states. *Science Advances* **8**(21), 7585 (2022)

- [34] Krause, A.G., Winger, M., Blasius, T.D., Lin, Q., Painter, O.: A high-resolution microchip optomechanical accelerometer. *Nature Photonics* **6**(11), 768–772 (2012)
- [35] Singh, R., Cole, G.D., Cripe, J., Corbitt, T.: Stable optical trap from a single optical field utilizing birefringence. *Phys. Rev. Lett.* **117**, 213604 (2016) <https://doi.org/10.1103/PhysRevLett.117.213604>
- [36] Cripe, J., Aggarwal, N., Lanza, R., Libson, A., Singh, R., Heu, P., Follman, D., Cole, G.D., Mavalvala, N., Corbitt, T.: Measurement of quantum back action in the audio band at room temperature. *Nature* **568**(7752), 364–367 (2019) <https://doi.org/10.1038/s41586-019-1051-4>
- [37] Cripe, J.: Broadband measurement and reduction of quantum radiation pressure noise in the audio band. PhD thesis, Louisiana State University Libraries (2018). https://doi.org/10.31390/gradschool_dissertations.4653 . http://dx.doi.org/10.31390/gradschool_dissertations.4653
- [38] Aggarwal, N., Cullen, T.J., Cripe, J., Cole, G.D., Lanza, R., Libson, A., Follman, D., Heu, P., Corbitt, T., Mavalvala, N.: Room-temperature optomechanical squeezing. *Nature Physics* **16**(7), 784–788 (2020)
- [39] Aggarwal, N.: A room temperature optomechanical squeezer (2020) <https://doi.org/10.48550/ARXIV.2006.14323>
- [40] Cripe, J., Aggarwal, N., Singh, R., Lanza, R., Libson, A., Yap, M.J., Cole, G.D., McClelland, D.E., Mavalvala, N., Corbitt, T.: Radiation-pressure-mediated control of an optomechanical cavity. *Phys. Rev. A* **97**, 013827 (2018) <https://doi.org/10.1103/PhysRevA.97.013827>
- [41] Whittle, C., Hall, E.D., Dwyer, S., Mavalvala, N., Sudhir, V., *et al.*: Approaching

the motional ground state of a 10-kg object. *Science* **372**(6548), 1333 (2021)

- [42] Lane, B.B.: Conditional mechanical squeezing of a micromechanical oscillator approaching the quantum regime. PhD thesis, Massachusetts Institute of Technology (2024)
- [43] Ganapathy, D., Jia, W., Nakano, M., Xu, V., Aritomi, N., Cullen, T., Kijbunchoo, N., Dwyer, S.E., Mullavey, A., McCuller, L., Abbott, R., Abouelfettouh, I., Adhikari, R.X., Ananyeva, A., Appert, S., Arai, K., Aston, S.M., Ball, M., Ballmer, S.W., Barker, D., Barsotti, L., Berger, B.K., Betzwieser, J., Bhattacharjee, D., Billingsley, G., Biscans, S., Bode, N., Bonilla, E., Bossilkov, V., Branch, A., Brooks, A.F., Brown, D.D., Bryant, J., Cahillane, C., Cao, H., Capote, E., Clara, F., Collins, J., Compton, C.M., Cottingham, R., Coyne, D.C., Crouch, R., Csizmazia, J., Dartez, L.P., Demos, N., Dohmen, E., Driggers, J.C., Effler, A., Ejlli, A., Etzel, T., Evans, M., Feicht, J., Frey, R., Frischhertz, W., Fritschel, P., Frolov, V.V., Fulda, P., Fyffe, M., Gateley, B., Giaime, J.A., Giardina, K.D., Glanzer, J., Goetz, E., Goetz, R., Goodwin-Jones, A.W., Gras, S., Gray, C., Griffith, D., Grote, H., Guidry, T., Hall, E.D., Hanks, J., Hanson, J., Heintze, M.C., Helmling-Cornell, A.F., Holland, N.A., Hoyland, D., Huang, H.Y., Inoue, Y., James, A.L., Jennings, A., Karat, S., Karki, S., Kasprzack, M., Kawabe, K., King, P.J., Kissel, J.S., Komori, K., Kontos, A., Kumar, R., Kuns, K., Landry, M., Lantz, B., Laxen, M., Lee, K., Lesovsky, M., Llamas, F., Lormand, M., Loughlin, H.A., Macas, R., MacInnis, M., Makarem, C.N., Mannix, B., Mansell, G.L., Martin, R.M., Mason, K., Matichard, F., Mavalvala, N., Maxwell, N., McCarrol, G., McCarthy, R., McClelland, D.E., McCormick, S., McRae, T., Mera, F., Merilh, E.L., Meylahn, F., Mittleman, R., Moraru, D., Moreno, G., Nelson, T.J.N., Neunzert, A., Notte, J., Oberling, J., O’Hanlon, T., Osthelder, C., Ottaway, D.J., Overmier, H., Parker, W., Pele, A., Pham, H., Pirello, M.,

- Quetschke, V., Ramirez, K.E., Reyes, J., Richardson, J.W., Robinson, M., Rollins, J.G., Romel, C.L., Romie, J.H., Ross, M.P., Ryan, K., Sadecki, T., Sanchez, A., Sanchez, E.J., Sanchez, L.E., Savage, R.L., Schaetzl, D., Schiworski, M.G., Schnabel, R., Schofield, R.M.S., Schwartz, E., Sellers, D., Shaffer, T., Short, R.W., Sigg, D., Slagmolen, B.J.J., Soike, C., Soni, S., Srivastava, V., Sun, L., Tanner, D.B., Thomas, M., Thomas, P., Thorne, K.A., Torrie, C.I., Traylor, G., Ubhi, A.S., Vajente, G., Vanosky, J., Vecchio, A., Veitch, P.J., Vibhute, A.M., Reis, E.R.G., Warner, J., Weaver, B., Weiss, R., Whittle, C., Willke, B., Wipf, C.C., Yamamoto, H., Zhang, L., Zucker, M.E.: Broadband quantum enhancement of the ligo detectors with frequency-dependent squeezing. *Phys. Rev. X* **13**, 041021 (2023) <https://doi.org/10.1103/PhysRevX.13.041021>
- [44] Graham, P.W., Kaplan, D.E., Mardon, J., Rajendran, S., Terrano, W.A.: Dark matter direct detection with accelerometers. *Physical Review D* **93**(7), 075029 (2016)
- [45] Komori, K., Ďurovčíková, D., Sudhir, V.: Quantum theory of feedback cooling of an anelastic macromechanical oscillator. *Phys. Rev. A* **105**, 043520 (2022) <https://doi.org/10.1103/PhysRevA.105.043520>
- [46] Groeblacher, S., Trubarov, A., Prigge, N., Cole, G., Aspelmeyer, M., Eisert, J.: Observation of non-markovian micromechanical brownian motion. *Nature communications* **6**(1), 7606 (2015)
- [47] González, G.I., Saulson, P.R.: Brownian motion of a torsion pendulum with internal friction. *Physics Letters A* **201**(1), 12 (1995) [https://doi.org/10.1016/0375-9601\(95\)00194-8](https://doi.org/10.1016/0375-9601(95)00194-8)
- [48] Kajima, M., Kusumi, N., Moriwaki, S., Mio, N.: Wide-band measurement of mechanical thermal noise using a laser interferometer. *Physics Letters A* **264**(4),

- 251 (1999) [https://doi.org/10.1016/S0375-9601\(99\)00828-2](https://doi.org/10.1016/S0375-9601(99)00828-2)
- [49] Neben, A.R., Bodiya, T.P., Wipf, C., Oelker, E., Corbitt, T., Mavalvala, N.: Structural thermal noise in gram-scale mirror oscillators. *New Journal of Physics* **14**(11), 115008 (2012) <https://doi.org/10.1088/1367-2630/14/11/115008>
- [50] Callen, H., Welton, T.: Irreversibility and generalized noise. *Physical Review* **83**, 34 (1951)
- [51] Kubo, R.: The fluctuation-dissipation theorem. *Reports on Progress in Physics* **29**(1), 255 (1966) <https://doi.org/10.1088/0034-4885/29/1/306>
- [52] Saulson, P.R.: Thermal noise in mechanical experiments. *Phys. Rev. D* **42**, 2437–2445 (1990) <https://doi.org/10.1103/PhysRevD.42.2437>
- [53] Zener, C.: Internal friction in solids. *Proceedings of the Physical Society* **52**(1), 152 (1940) <https://doi.org/10.1088/0959-5309/52/1/322>